# MODELING OF NANOTUBE-REINFORCED POLYMER COMPOSITES
# AFOSR GRANT F49620-03-1-0442

**Xin-Lin Gao**
Department of Mechanical Engineering-Engineering Mechanics,
Michigan Technological University, Houghton, MI 49931-1295
(Currently at Department of Mechanical Engineering, Texas A&M University,
3123 TAMU, College Station, TX 77843-3123
Tel: (979) 845-4835 Fax: (979) 845-3081 E-mail: xlgao@tamu.edu)

## Final Report

Carbon nanotubes have been identified as promising reinforcing materials for high-performance nanocomposites (e.g., Thostenson et al., 2001; Maruyama and Alam, 2002). Reliable structural applications of carbon nanotube-reinforced composites depend on accurate understanding of their mechanical behavior. Efforts have been made to characterize the mechanical properties of the said nanocomposites. These studies, being typically based on experimental measurements or molecular dynamics simulations, tend to be expensive and configuration/material specific. The use of continuum-based models can mitigate these difficulties (e.g., Odegard et al., 2002; Li and Chou, 2003a; Gao and Li, 2003) and is, therefore, very desirable. The goal of the current research project is to explore continuum-based models for predicting effective elastic properties of and describing interfacial load transfer in carbon nanotube-reinforced polymer composites.

A continuum-based micromechanics model has been proposed (see Li et al. (2004) for details). Two steps are involved in the modeling procedure for two different length scales. In the first step, which is at the nanometer scale, a single walled carbon nanotube (SWCNT), the non-bulk polymer adjacent to the nanotube, and the nanotube/polymer interfacial layer are collectively treated as an effective continuum fiber (isotropic or transversely isotropic), whose effective elastic properties are determined by using an equivalent-continuum modeling method (Odegard et al., 2002). In the second step, which is at the micron scale, the Mori-Tanaka method restructured by Tandon and Weng (1984, 1986) and Qiu and Weng (1990) is used to predict the effective elastic properties of the SWCNT-reinforced polymer composites. As a parametric study, four nanocomposite systems, two transversely isotropic ones containing unidirectionally aligned nanotubes and two isotropic ones having randomly oriented nanotubes, are considered. Nanotube aspect ratio (AR), nanotube volume fraction ($c_1$) and nanotube orientation are chosen as three controlling parameters. Thermoplastic polyimide LaRc-SI with a 3% molecular weight offset is taken as the isotropic matrix material. Its Young's modulus and Poisson's ratio are, respectively, $E_0$ = 3.8 GPa and $\nu_0$ = 0.4 (Whitley et al., 2000). For the transversely isotropic effective fiber the five independent elastic stiffness constants are, respectively, taken to be $C_{11}$ = 457.6 GPa, $C_{12}$ = 8.4 GPa, $C_{22}$ = 14.3 GPa, $C_{23}$ = 5.5 GPa, $C_{44}$ = 27.0 GPa (Odegard et al., 2003). For the isotropic effective fiber the Young's modulus ($E_1$) and Poisson's ratio ($\nu_1$) are, respectively, regarded to be the same as the

longitudinal Young's modulus and Poisson's ratio of the transversely isotropic effective fiber, i.e., $E_1 = E_{11}^f = 450.4$ GPa, $\nu_1 = \nu_{12}^f = 0.42$, where $E_{11}^f$ and $\nu_{12}^f$ can be obtained from the stiffness constants given above. The effective fiber is assumed to have the same length as that of the nanotube, and the nanotube volume fraction ($c_1$) is taken to be 34% of the effective fiber volume fraction (Odegard et al., 2003).

For the transversely isotropic composites containing unidirectionally aligned isotropic nanotubes, numerical results show that when AR increases the effective longitudinal Young's modulus $E_{11}$ increases, while the effective Poisson's ratio $\nu_{12}$ decreases, both in a monotonic manner (see Figs. 1 and 2). Furthermore, with the increase of AR, $E_{11}$ approaches, while $\nu_{12}$ deviates from, their corresponding results predicted by the rule of mixtures (e.g., Chawla, 1993) according to:

$$E_{11} = E_0 + (E_1 - E_0)\, c_1/0.34, \tag{1}$$

$$\nu_{12} = \nu_0 + (\nu_1 - \nu_0)\, c_1/0.34. \tag{2}$$

In addition, $\nu_{12}$ increases with $c_1$ when AR is small, but decreases with $c_1$ when AR is getting close to 25. When isotropic nanotubes are randomly oriented in the polymer matrix, the effective Young's modulus $E$ of the resulting isotropic composites increases with both AR and $c_1$, while the opposite trend is observed for the effective Poisson's ratio $\nu$ (see Figs. 3 and 4). By comparing Fig. 1 with Fig. 3 and Fig. 2 with Fig. 4, one can see that the values of $E$ and $\nu$ are smaller than their corresponding values of $E_{11}$ and $\nu_{12}$ for the same values of AR and $c_1$, as expected.

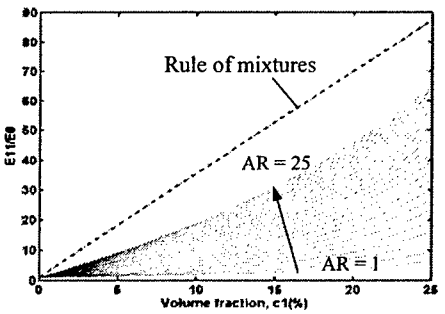


Fig. 1. Aligned SWCNTs (isotropic).

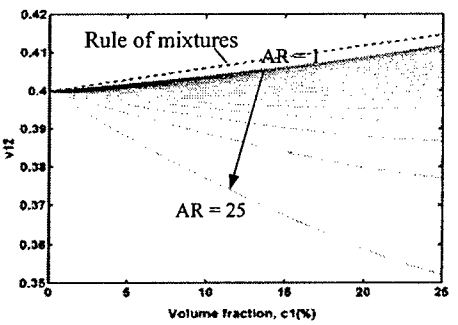


Fig. 2. Aligned SWCNTs (isotropic).

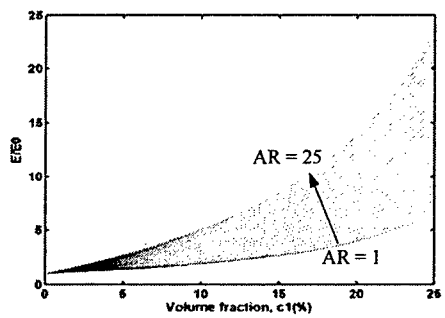


Fig. 3. Random SWCNTs (isotropic).

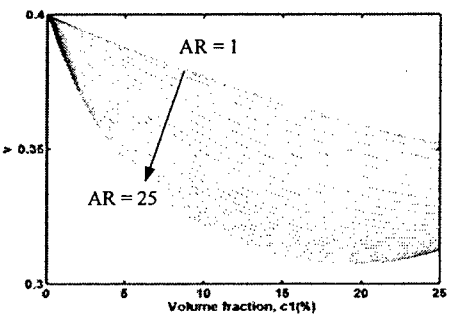


Fig. 4. Random SWCNTs (isotropic).

For the nanocomposites reinforced by transversely isotropic nanotubes, the trends of the Young's modulus and Poisson's ratio varying with AR and $c_1$ (see Figs. 5 – 8) are similar to those for the nanocomposites containing isotropic nanotubes (see Figs. 1 – 4). An exception is that the Poisson's ratio ($\nu$) for isotropic nanocomposites reinforced by randomly oriented transversely isotropic nanotubes (see Fig. 8) decreases monotonically with the increase of $c_1$, which differs from what is exhibited by isotropic nanocomposites reinforced by randomly oriented isotropic nanotubes (see Fig. 4).

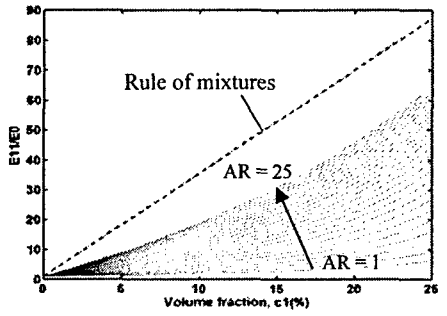


Fig. 5. Aligned SWCNTs (transversely isotropic).

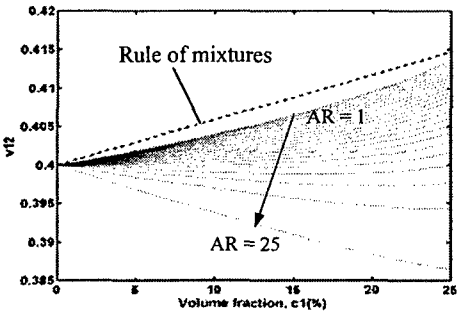


Fig. 6. Aligned SWCNTs (transversely isotropic).

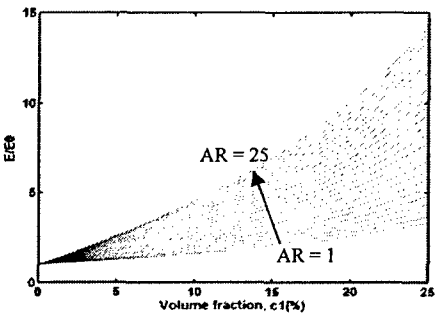


Fig. 7. Random SWCNTs (transversely isotropic).

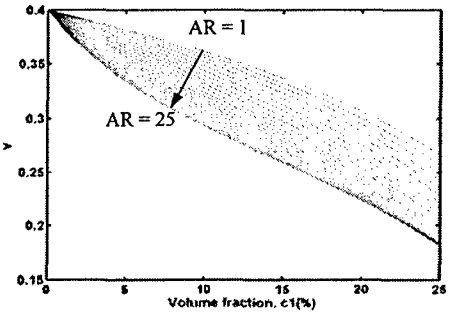


Fig. 8. Random SWCNTs (transversely isotropic).

The stress transfer problem for traditional fiber-reinforced composites has been extensively studied. The shear-lag model originally proposed by Cox (1952) provides a good estimate of the stresses in the fiber transferred from the matrix through the interface. However, this analytical model cannot be directly applied to characterize nanotube-reinforced composites, since it considers the load transfer across the curved interface only and regards the fiber ends as traction-free. In addition, some important morphological features of nanotube-reinforced composites are not incorporated in existing shear-lag models. It is known that the efficiency of the nanotube reinforcement depends sensitively on the morphology (including diameter, wall thickness and chirality) and distribution of the nanotubes (e.g., Thostenson and Chou, 2003). This necessitates the incorporation of atomistic structures of nanotubes in developing continuum-based analytical models of shear-lag type for nanotube-reinforced composites. One objective of the current project is to develop such a shear-lag model using a representative volume element (RVE) of a concentric composite cylinder embedded with a capped carbon

nanotube (see Fig. 9(b)). The molecular structural mechanics of Li and Chou (2003a) is first employed to predict the effective Young's modulus of the capped nanotube. The capped nanotube is then replaced by an effective (solid) fiber, whose length and diameter are kept to be the same as those of the nanotube to preserve the essential morphological features of the nanocomposite (see Fig. 9(c)). The Young's modulus of the effective fiber is subsequently determined under an isostrain condition. This is followed by the development of the shear-lag model using the cylindrical RVE shown in Fig. 9(c).

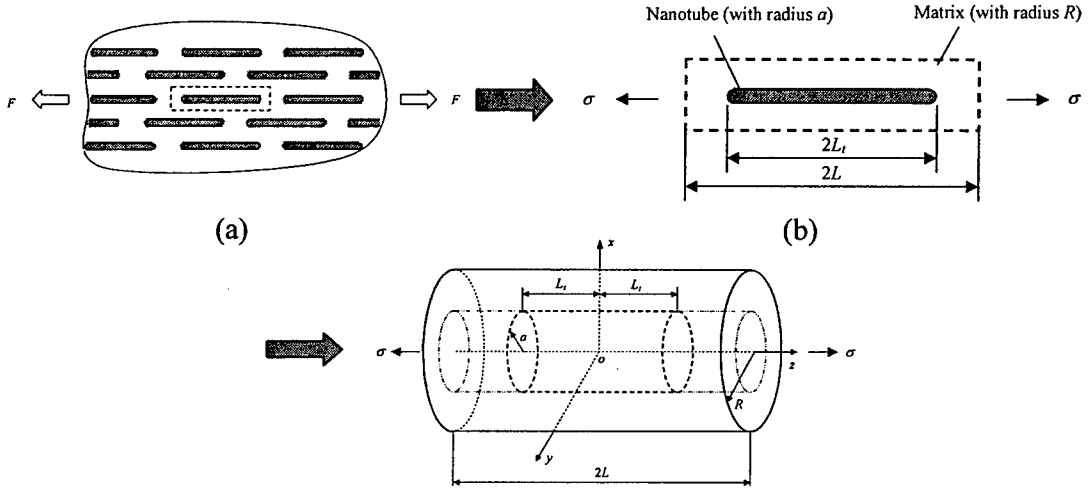


Fig. 9. Representative volume element.

The formulation of the shear-lag model is based on the elasticity theory for axisymmetric problems. The major assumptions are typical of a shear-lag analysis. The results give (see Gao and Li (2005) for details)

$$\overline{\sigma_{zz}^f} = \left\{ \frac{R^2}{a^2 + \frac{E^m}{E^f}\left(R^2 - a^2\right)} + \left[ 1 - \frac{R^2}{a^2 + \frac{E^m}{E^f}\left(R^2 - a^2\right)} \right] \frac{\cosh(\alpha z)}{\cosh(\alpha L_t)} \right\} \sigma,$$

$$\tau_i = \frac{a\alpha \sinh(\alpha z)}{2\cosh(\alpha L_t)} \frac{\left(R^2 - a^2\right)\left(1 - \frac{E^m}{E^f}\right)}{a^2 + \frac{E^m}{E^f}\left(R^2 - a^2\right)} \sigma, \quad \tau_{rz}^f = \frac{r\alpha \sinh(\alpha z)}{2\cosh(\alpha L_t)} \frac{\left(R^2 - a^2\right)\left(1 - \frac{E^m}{E^f}\right)}{a^2 + \frac{E^m}{E^f}\left(R^2 - a^2\right)} \sigma,$$

$$\tau_{rz}^m = \frac{\alpha \sinh(\alpha z)}{2\cosh(\alpha L_t)} \frac{a^2\left(1 - \frac{E^m}{E^f}\right)}{a^2 + \frac{E^m}{E^f}\left(R^2 - a^2\right)} \left( \frac{R^2}{r} - r \right) \sigma.$$

$$\sigma_{zz}^{m}=\frac{\left[R^2\ln\frac{r}{a}-\frac{1}{2}\left(r^2-a^2\right)\right]R^2}{R^4\ln\frac{R}{a}-\frac{1}{4}\left(R^2-a^2\right)\left(3R^2-a^2\right)}\sigma+\left\{\frac{E^m}{E^f}-\frac{\left[a^2+\frac{E^m}{E^f}\left(R^2-a^2\right)\right]\left[R^2\ln\frac{r}{a}-\frac{1}{2}\left(r^2-a^2\right)\right]}{R^4\ln\frac{R}{a}-\frac{1}{4}\left(R^2-a^2\right)\left(3R^2-a^2\right)}\right\}$$
$$\times\left\{\frac{R^2}{a^2+\frac{E^m}{E^f}\left(R^2-a^2\right)}+\left[1-\frac{R^2}{a^2+\frac{E^m}{E^f}\left(R^2-a^2\right)}\right]\frac{\cosh(\alpha z)}{\cosh(\alpha L_t)}\right\}\sigma. \quad (3)$$

By using the shear-lag formulas given in Eq. (3), sample numerical results are readily obtained. Fig. 10 shows how the normalized interfacial shear stress and average axial normal stress in the nanotube vary along the nanotube length for three cases having different nanotube aspect ratios (ARs). A comparison shows that in all of the three cases (with different aspect ratios) considered the trends of both $\tau_i/\sigma$ and $\overline{\sigma_{zz}^f}/\sigma$ varying with $z/(2a)$, as predicted by the current shear-lag model, are the same as those predicted by the earlier computational model of Li and Chou (2003b), thereby verifying the new model.

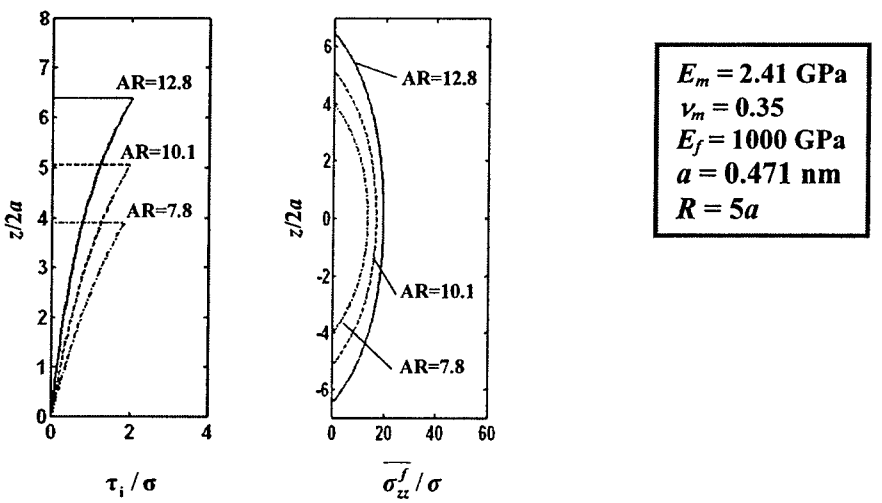


Fig. 10. Interfacial shear stress and average axial normal stress in the nanotube.

Fig. 11 shows the distribution of the average axial normal stress in the nanotube along the nanotube length, while Fig. 12 illustrates that of the average axial normal stress in the matrix. Clearly, it is observed from Fig. 11 that the maximum axial normal stress is reached in the middle of the nanotube, whereas the minimum occurs at its two ends. Also, it is seen that the larger the aspect ratio, the higher the average axial normal stress at the same $z$ for given $a$ and $\sigma$. The opposite trends are seen for the average normal stress in the matrix, as shown in Fig. 12. More importantly, it can be noticed from comparing Figs. 11 and 12 that when the nanotube aspect ratio is sufficiently large, most of the applied load in the axial direction can be taken up by the nanotube and the surrounding matrix needs to support only a small portion of the axial loading. For example, when AR = 12.8 the portion of the applied load taken by the nanotube on the cross section $z = 0$ is more than three times as large as that by the matrix on the same cross section, although the cross-sectional area of the matrix is twenty-four times as big as that of the effective fiber on $z = 0$ in the current RVE with $R = 5a$. However, this is no longer the case if the nanotube aspect ratio becomes small. For instance, when AR = 7.8 both of the nanotube

and the matrix on the cross section $z = 0$ take about the equal amount of the applied load. These reveal that the nanotube aspect ratio is a critical controlling parameter for nanotube-reinforced composites, and that for significant reinforcements nanotubes with large aspect ratios should be used. This observation conforms to what has been found in existing experimental and computational studies (e.g., Frankland et al., 2003), thereby further supporting the newly developed analytical model.

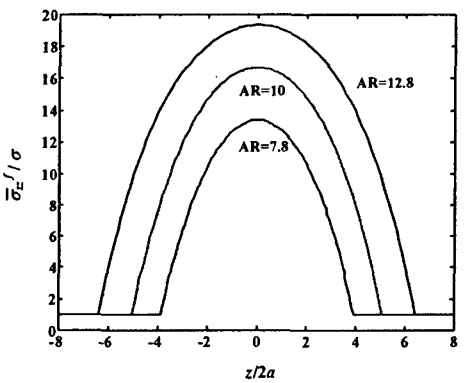


Fig. 11. Average axial normal stress in the nanotube.

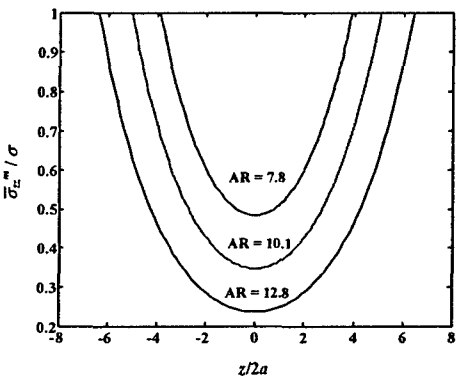


Fig. 12. Average axial normal stress in the matrix.

## References


Chawla, K. K., 1993, *Ceramic Matrix Composites*, Chapman & Hall, London.

Cox, H. L., 1952, The elasticity and strength of paper and other fibrous materials, *Brit. J. Appl. Phys.* **3**, 72-79.

Frankland, S. J. V., Harik, V. M., Odegard, G. M., Brenner, D. W. and Gates, T. S., 2003, The stress-strain behavior of polymer-nanotube composites from molecular dynamics simulation, *Compos. Sci. Tech.* **63**, 1655-1661.

Gao, X.-L. and Li, K., 2003, Finite deformation continuum model for single-walled carbon nanotubes, *Int. J. Solids Struct.* **40**, 7329-7337.

Gao, X.-L. and Li, K., 2005, A Shear-lag model for carbon nanotube-reinforced polymer composites, *Int. J. Solids Struct.* **42**, 1649-1667.

Li, C. and Chou, T.-W., 2003a, A structural mechanics approach for the analysis of carbon nanotubes, *Int. J. Solids Struct.* **40**, 2487-2499.

Li, C. and Chou, T.-W., 2003b, Multiscale modeling of carbon nanotube reinforced polymer composites, *J. Nanosci. Nanotech.* **3**, 1-8.

Li, K., Gao, X.-L. and Roy, A. K., 2004, Micromechanical modeling of carbon nanotube-reinforced polymer composites, in *Proc. of the 11th Int. Conf. on Composites/Nano Engineering* (ICCE-11), Hilton-Head, SC, August 8-14, 2004.

Maruyama, B. and Alam, K., 2002, Carbon nanotubes and nanofibers in composite materials, *SAMPE Journal* **38**(3), 59-68.

Odegard, G. M., Gates, T. S., Nicholson, L. M. and Wise, K. E., 2002, Equivalent-continuum modeling of nano-structured materials, *Compos. Sci. Tech.* **62**, 1869-1880.

Odegard, G. M., Gates, T. S., Wise, K. E., Park, C. and Siochi, E. J., 2003, Constitutive modeling of nanotube-reinforced polymer composites, *Compos. Sci. Tech.* **63**, 1671-1687.

Qiu, Y. P. and Weng, G. J., 1990, On the application of Mori-Tanaka's theory involving transversely isotropic spheroidal inclusions, *Int. J. Engng. Sci.* **28**, 1121-1137.

Tandon, G. P. and Weng, G. J., 1984, Effect of aspect ratio of inclusions on the elastic properties of unidirectionally aligned composites, *Polym. Compos.* **5**, 327-333.

Tandon, G. P. and Weng, G. J., 1986, Average stress in the matrix and effective moduli of randomly oriented composites, *Compos. Sci. Tech.* **27**, 111-132.

Thostenson, E. T. and Chou, T.-W., 2003, On the elastic properties of carbon nanotube-based composites: modeling and characterization, *J. Phys. D: Appl. Phys.* **36**, 573-582.

Thostenson, E. T., Ren, Z. and Chou, T.-W., 2001, Advances in the science and technology of carbon nanotubes and their composites: a review, *Compos. Sci. Tech.* **61**, 1899-1912.

Whitley, K. S., Gates, T. S., Hinkley, J. A. and Nicholson, L. M., 2000, Mechanical properties of LaRC$^{TM}$SI polymer for a range of molecular weights, NASA/TM-2000-210304.

Lee

# REPORT DOCUMENTATION PAGE

AFRL-SR-AR-TR-05-

0293



| 1. REPORT DATE (DD-MM-YYYY) | 2. REPORT TYPE | 3. DATES COVERED (From - To) |
|---|---|---|
| 04-20-2005 | Final | Sept 2003 - Sept 2004 |

**4. TITLE AND SUBTITLE**
Modeling of Nanotube-Reinforced Polymer Composites

**5a. CONTRACT NUMBER**
F49620-03-1-0442

**5b. GRANT NUMBER**

**5c. PROGRAM ELEMENT NUMBER**

**6. AUTHOR(S)**
Xin-Lin Gao

**5d. PROJECT NUMBER**

**5e. TASK NUMBER**

**5f. WORK UNIT NUMBER**

**7. PERFORMING ORGANIZATION NAME(S) AND ADDRESS(ES)**

Michigan Tech. University
1400 Townsend Drive
Houghton, MI 49931-1295

**8. PERFORMING ORGANIZATION REPORT NUMBER**

MTU Proposal # 030918

**9. SPONSORING / MONITORING AGENCY NAME(S) AND ADDRESS(ES)**

AF Office of Sci. Research
4015 Wilson Blvd Room 713
Arlington, VA 22203-1954

NA

**10. SPONSOR/MONITOR'S ACRONYM(S)**
AFOSR

**11. SPONSOR/MONITOR'S REPORT NUMBER(S)**

**12. DISTRIBUTION / AVAILABILITY STATEMENT**

Approved for public release,
distribution unlimited

**13. SUPPLEMENTARY NOTES**

**14. ABSTRACT**

Carbon nanotubes have been identified as promising reinforcing materials for high-performance nanocomposites. Reliable structural applications of carbon nanotube-reinforced composites depend on accurate understanding of their mechanical behavior. Efforts have been made to characterize the mechanical properties of the said nanocomposites. These studies, being typically based on experimental measurements or molecular dynamics simulations, tend to be expensive and configuration/material specific. The use of continuum-based models can mitigate these difficulties and is, therefore, very desirable. Two continuum-based models were developed in the course of this project, one for predicting effective elastic properties of and the other for describing interfacial load transfer in carbon nanotube-reinforced polymer composites.

**15. SUBJECT TERMS**
Carbon Nanotube; Polymer Matrix; Nanocomposites; Effective Elastic Properties; Stress Transfer; Mori-Tanaka Method; Shear-Lag Model

| 16. SECURITY CLASSIFICATION OF: | | | 17. LIMITATION OF ABSTRACT | 18. NUMBER OF PAGES | 19a. NAME OF RESPONSIBLE PERSON |
|---|---|---|---|---|---|
| a. REPORT | b. ABSTRACT | c. THIS PAGE | | | Xin-Lin Gao |
| U | U | U | UU | 7 | 19b. TELEPHONE NUMBER (include area code) 979-845-4835 |



7-21-05